International Journal of Psychophysiology 97 (2015) 258–270

Contents lists available at ScienceDirect

International Journal of Psychophysiology

journal homepage: www.elsevier.com/locate/ijpsycho

Hemifield-dependent N1 and event-related theta/delta oscillations: An unbiased comparison of surface Laplacian and common EEG reference choices

Jürgen Kayser *, Craig E. Tenke

Division of Cognitive Neuroscience, New York State Psychiatric Institute, New York, NY, USA
Department of Psychiatry, Columbia University College of Physicians & Surgeons, New York, NY, USA

ARTICLE INFO

Article history:
Received 13 August 2014
Received in revised form 17 November 2014
Accepted 21 December 2014
Available online 3 January 2015

Keywords:
Current source density (CSD)
EEG recording reference
Event-related potentials (ERPs)
Event-related spectral perturbations (ERSPs)
Principal components analysis (PCA)
Visual half-field (VHF) paradigm
N1pc
Signal-to-noise
Sample size
Time-frequency analysis
ERS/ERD
Reference electrode standardization technique (REST)
Volume conduction
Surface Laplacian
Permutation tests

ABSTRACT

Surface Laplacian methodology has been used to reduce the impact of volume conduction and arbitrary choice of EEG recording reference for the analysis of surface potentials. However, the empirical implications of employing these different transformations to the same EEG data remain obscure. This study directly compared the statistical effects of four commonly-used (nose, linked mastoids, average) or recommended (reference electrode standardization technique [REST]) references and their spherical spline current source density (CSD) transformation for a large data set stemming from a well-understood experimental manipulation. ERPs (72 sites) recorded from 130 individuals during a visual half-field paradigm with highly-controlled emotional stimuli were characterized by mid-parietooccipital N1 (125 ms peak latency) and event-related synchronization (ERS) of theta/delta (160 ms), which were most robust over the contralateral hemisphere. All five data transformations were rescaled to the same covariance and submitted to a single temporal or time-frequency PCA (Varimax) to yield simplified estimates of N1 or theta/delta ERS. Unbiased nonparametric permutation tests revealed that these hemifield-dependent asymmetries were by far most focal and prominent for CSD data, despite all transformations showing maximum effects at mid-parietooccipital sites. Employing smaller subsamples (signal-to-noise) or window-based ERP/ERS amplitudes did not affect these comparisons. Furthermore, correlations between N1 and theta/delta ERS at these sites were strongest for CSD and weakest for nose-referenced data. Contrary to the common notion that the spatial high pass filter properties of a surface Laplacian reduce important contributions of neuronal generators to the EEG signal, the present findings demonstrate that instead volume conduction inherent in surface potentials weakens the representation of neuronal activation patterns at scalp that directly reflect regional brain activity.

1. Introduction

1.1. EEG surface potentials need a reference

Ranking among the most popular research tools of cognitive neuroscience, event-related potentials and oscillations (ERPs and EROs) measure time-locked field potentials in time and time-frequency domains. Because the underlying data are extracted from the scalp-recorded electroencephalogram (EEG), these tools are subject to using an EEG recording reference, a necessary prerequisite for recording surface potentials. This requirement is in stark contrast to analogous measures derived from magnetoencephalography (MEG) recordings, which, although less cost-effective than their EEG counterparts, also enable studying neuronal activity and human cognition within a millisecond time resolution (e.g., Keil et al., 2014). Because the EEG signal must be quantified as a potential difference between any two recording sites, the properties of the reference have a fundamental impact on any measure derived from the EEG (e.g., Kayser and Tenke, 2010). Unfortunately, a "neutral" or even "quiet" reference location does not exist anywhere on the human body, because the EEG, as all electrical signals, is instantaneously volume-conducted throughout all physiological tissues. While this renders all choices for an EEG recording reference inherently arbitrary, the field has nevertheless developed a preferential use of different reference schemes, including linked ear lobes or mastoids, nose tip, or the common average of all recording sites. If dense-electrode arrays (i.e., 64, 128 or more EEG channels) enable high spatial sampling to sufficiently cover the original signal space, that is, a closed surface containing all current within its volume, the use of an average reference has been advocated because, in this case, the sum of all recorded EEG activity will

* Corresponding author at: New York State Psychiatric Institute, Division of Cognitive Neuroscience, Unit 50, 1051 Riverside Drive, New York, NY 10032, USA. Tel.: +1 646 774 5207; fax: +1 212 543 6540.
E-mail address: kayserj@nyspi.columbia.edu (J. Kayser).

http://dx.doi.org/10.1016/j.ijpsycho.2014.12.011
0167-8760/

approximate zero (i.e., an inactive reference; e.g., Bertrand et al., 1985). However, spatial sampling from the ventral side of the brain is a practical impossibility and the uneven spatial sampling across the surface of (brain) current volume produces a bias toward the center of the EEG montage (Junghöfer et al., 1999). Despite these recognized limitations, the average reference is widely considered to be superior to all other known reference schemes (e.g., Dien, 1998; Nunez and Srinivasan, 2006), even for lower-density EEG montages, because it is independent of any particular recording sites included in the EEG montage. In theory, sparse electrode sampling could be compensated by employing spherical splines to interpolate EEG data for an improved estimate of the average reference (Ferree, 2006), but this has rarely been done in practice.

As an alternative to the average reference, Yao (2001) proposed a reference electrode standardization technique (REST) that estimates the theoretical EEG reference at infinity from the observed (i.e., referenced) surface potentials. REST involves the computation of a (non-unique) equivalent dipole source solution based on a large number of radial dipoles, however, not to provide an EEG inverse solution, which is always undetermined, but to obtain a reference standardization or transfer matrix that is independent of the actual neuronal generators. An extension of this idea involving analytical expressions for the transfer matrix has been formulated by Thuraisingham (2011), which provides several computational advantages. However, for any given EEG montage, the transfer matrix has to be computed only once and can then be used to obtain, via basic linear algebra, an estimate of the infinite reference. Unlike other reference schemes, this estimate is unique; however, like any other reference scheme, it is also a constant that is subtracted from all recording sites to rereference surface potentials to infinity. Several studies have found that REST performs favorably in comparison with other reference schemes when analyzing EEG spectra (Qin et al., 2010; Yao et al., 2005), EEG coherence (Marzetti et al., 2007) or ERPs (Yao et al., 2007). However, several caveats of REST in direct comparison with the average reference have been stipulated, including the fictional conceptualization of measuring scalp potentials with respect to "infinity" and questions about the head model accuracy/uncertainty (Nunez, 2010).

The surface Laplacian, also synonymously called scalp current density (SCD) or current source density (CSD), is often used to transform reference-dependent surface potentials into estimates of radial current flow at cortex or scalp (e.g., Nunez and Westdorp, 1994). Acting as spatial high pass filter (second spatial derivative), it yields sharper topographies compared to those of scalp potentials (e.g., Nunez and Srinivasan, 2006). At the same time, the value of the surface Laplacian is not restricted to its mathematical filter properties but is related to physical principles rendering a unique, *reference-free* representation of current generators underlying an EEG topography that has – unlike surface potentials – physical meaning (Carvalhaes and de Barros, 2015; Tenke and Kayser, 2012). Despite the recognized theoretical advantages of the surface Laplacian, EEG researchers at large have been surprisingly reluctant to embrace these methods in their research, partly because direct comparisons and simulation studies are scarce (e.g., Kayser and Tenke, 2006a; Nunez et al., 1997, 1999). One often cited concern is the purported susceptibility of the surface Laplacian to increased noise levels (e.g., Bradshaw and Wikswo, 2001), or a low signal-to-noise ratio, because its computation is inherently based on signal differences (i.e., second spatial derivative; for a primer, see Kayser and Tenke, in revision). However, the surface Laplacian can also increase the signal-to-noise ratio by reducing spatial noise due to volume conduction (e.g., McFarland, 2014; Tenke and Kayser, 2012). If there is a real trade-off between the use of surface Laplacian and scalp potentials (e.g., Giard et al., 2014; Nunez and Srinivasan, 2006; Srinivasan et al., 1998), it should be quantified and submitted to a cost–benefit analysis.

1.2. The present study

Given the scarcity of systematic comparisons of how a particular choice of EEG reference affects the statistical outcome of a study, and even rarer reports including a surface Laplacian as reference-free technique in such a comparison, the present study sought to compare three common reference schemes (i.e., nose, linked mastoids, and average reference), an estimate of the 'infinite' reference (REST; Yao, 2001), and spherical spline CSD estimates (Pascual-Marqui et al., 1988; Perrin et al., 1989) using ERP and ERO measures obtained in a visual half-field (VHF) paradigm. The VHF technique exploits the functional neuroanatomy of the visual system, in which the afferent projections from the nasal sides of each retina cross in the optic chiasm to the contralateral hemisphere. This yields a divided representation of the two hemifields in primary visual cortex, with the left visual field (LVF) projecting to the right hemisphere (RH), and, vice versa, the right visual field (RVF) to the left hemisphere (LH). This division by hemifield is exclusive provided that the visual stimulus is presented sufficiently outside the foveal field ($\pm 1.5°$ horizontal eccentricity), which has bihemispheric projections (e.g., McKeever, 1986; Young, 1982); however, interhemispheric transfer may nevertheless be necessary for optimal decoding of foveally-presented stimuli (e.g., Van der Haegen et al., 2013). While this paradigm has been extensively used in studies of functional hemispheric asymmetry (e.g., Springer and Deutsch, 1981), it is often also implicitly embedded in cognitive tasks of visual attention (e.g., Casiraghi et al., 2013; Eimer, 1996; Verleger et al., 2012). Its relevance for the present purpose, that is, comparing the effectiveness of different spatial transformations of EEG data for uncovering ERP and ERO effects with regard to an experimental manipulation, stems from the distinct asymmetrical representation of visual information in striate and extrastriate cortices, which primarily contributes to the generation of early visual ERP components. Clark et al. (1995) carefully investigated the generators of early ERPs (50–250 ms) to checkerboard stimuli as a function of visual field position, and concluded that a negative posterior component contralateral to the stimulated hemifield (N1) appears to arise from multiple occipito-parietal and occipito-temporal generators, involving lateral extrastriate cortex and/or posterior temporal regions. Because of its prominence in visual ERP waveforms, this strongly lateralized component has also been used as a tool to estimate interhemispheric transfer times by calculating differences in N1 latency at ipsilateral and contralateral scalp sites (e.g., Endrass et al., 2002; Saron and Davidson, 1989; Whitford et al., 2011). Hence, the asymmetry of N1 amplitude as a function of hemifield stimulation (i.e., its focal, posterior contralateral representation within the N1 topography, which has also been termed N1pc; e.g., Verleger et al., 2012) may represent an ideal test case for the current objective because we can experimentally manipulate neuronal generator locations in the brain without resorting to simulations.

Evoked spectral power and stimulus-induced phase resetting of ongoing EEG rhythms, ranging from delta to beta frequencies, have been discussed as contributing mechanisms for the generation of ERP components, including visual N1 (e.g., Makeig et al., 2002; Klimesch et al., 2004; Gruber et al., 2005). While changes in neural oscillations are concealed by the ERP averaging process, a time-frequency decomposition of the single trials used to compute ERPs allows the quantification of event-related spectral changes over time (e.g., Makeig, 1993; Pfurtscheller and Lopes da Silva, 1999; Herrmann et al., 2014). To the extent that event-related oscillations contribute locally to the generation of N1pc, we hypothesize similar hemifield-dependent asymmetric EROs, presumably involving low frequencies in the theta and delta range, as previously observed for an auditory N1 (Kayser et al., 2014). Thus, a secondary goal was to study the association between theta/delta EROs and visual N1pc.

Consistent with our prior research, we employed a comprehensive approach for ERP and ERO analysis, which uses principal components analysis (PCA) to yield data-driven component estimates (e.g., Donchin and Heffley, 1978; Kayser and Tenke, 2003; Kayser et al., 2014; Tenke and Kayser, 2005). To further avoid any a priori assumptions typically required for statistical analysis, including independence of observations, normal distribution, homogeneity of variances, and preassigning scalp

sites to a repeated measures ANOVA design, topographic differences between hemifields were evaluated for each data transformation by means of unbiased randomization tests (e.g., Maris, 2004; Kayser et al., 2007, 2013). The impact of signal-to-noise ratio on these ERP and ERO measures was assessed by systematically reducing sample sizes and submitting these data to the same nonparametric permutation tests.

2. Material and methods

2.1. Participants

We analyzed the ERP data of 130 participants (58 male) between 13 and 64 years of age (*median* = 36.5), who were enrolled in an ongoing multiwave three-generation longitudinal study of individuals at high and low risk for major depression based on family history (Weissman et al., 1997, 2005, 2006). The sample was recruited from an urban setting (greater New Haven area, Connecticut, US), and consisted of Caucasian and working or middle class individuals. EEG testing was performed at the Psychophysiology Laboratory at New York State Psychiatric Institute (NYSPI). All procedures were approved by the institutional review boards at Yale University and at Columbia University/NYSPI. All participants gave written informed consent (≥18 years) or provided written assent (<18 years; written informed consent from parents).

2.2. Stimuli and procedure

The current visual half-field paradigm closely followed the procedures developed during prior studies (e.g., Kayser et al., 1997, 2000). Briefly, stimuli consisted of 16 closely-matched pairs of pictures depicting facial areas of patients with dermatological diseases *before* (negative) and *after* (neutral) surgical treatment. Hence, within each picture pair, neutral stimuli differ from negative stimuli only in the emotionally relevant feature but are virtually identical in all other aspects (i.e., their physical stimulus properties). Stimuli were presented as digitized images (resolution 182 × 137 pixels, 256 colors) on a 20-inch monitor (resolution 1280 × 1024 pixels) to the left or right hemifield on a light gray background in a light-dimmed, sound-attenuated IAC (Industrial Acoustics Company) booth. Using a chin rest attached to a desk, participants were positioned with their eyes at a constant 57 cm distance to the surface of the screen. A small black cross (20 × 20 pixels) in the middle of the screen served as fixation. Stimulus presentation subtended visual angles of 7.2° horizontally, with the outer borders at ±1.7° and ±8.9° from fixation in each visual field, and 5.4° vertically, centered along the fixation horizon. Stimulus exposure time was 250 ms. Rapid and predictable stimulus onsets and offsets were coordinated by STIM^2 software (NeuroScan, Inc., 2003b), and verified by direct measurement with a photo resistor attached to the surface of the screen.

Using a pseudo-randomized sequence of four blocks consisting of 32 trials (128 trials total), each stimulus was presented once per block to the left or right visual field. Within every four consecutive trials, each of the possible combinations of hemifield (left, right) and emotional content (negative, neutral) occurred exactly once, using stimuli from different stimulus pairs. Each participant received a different sequence. Because the affective feature of a particular stimulus was not necessarily in the center of the picture, stimuli were mirrored in blocks 3 and 4 (cf. Bryson et al., 1991). Stimuli were presented with variable inter-trial intervals (8–13 s). Trials were separated by the temporary disappearance of the fixation cross. Participants were instructed and trained to attend to the stimulus presentations while maintaining fixation, but allowed to relax between trials. No manual response was required.

2.3. Data acquisition, recording, and artifact procedures

Continuous EEGs were acquired at 1024 samples/s using a 24-bit BioSemi system (BioSemi, Inc., 2001) with a 72-channel scalp montage (Jurcak et al., 2007; Pivik et al., 1993) including the nose (Fig. 1). Data were screened for electrolyte bridges (Alschuler et al., 2014; Tenke and Kayser, 2001), exported to 16-bit Neuroscan format using Polyrex (Kayser, 2003) to apply a nose reference, remove DC offsets, filter low-frequency drifts (<0.0159 Hz = 10-s time constant) and optimize data scaling. Volume-conducted blink artifacts were removed from the raw EEG by spatial singular value decomposition (NeuroScan, Inc., 2003a). Bipolar vertical and horizontal EOGs were interpolated via spherical splines (Perrin et al., 1989).[1] Recording epochs of 1500 ms (200 ms prestimulus baseline) were extracted off-line and digitally low-pass filtered at 30 Hz (−24 dB/octave). Using a reference-free approach to identify residual artifacts on a channel-by-channel and trial-by-trial basis (Kayser and Tenke, 2006d), artifactual surface potentials were either replaced by spherical spline interpolation (Perrin et al., 1989) using the data from artifact-free channels (i.e., when less than 25% of all EEG channels contained an artifact) or the affected trial was rejected. Trials in which horizontal eye movements exceeded 2° from baseline before stimulus onset during stimulus exposure also were rejected. While our prior studies using this paradigm (Kayser et al., 1997, 2000) also excluded the matched stimulus presentations of a rejected trial (i.e., all four trials of a particular negative/neutral stimulus pair during blocks 1 and 2 or blocks 3 and 4), the current study estimated the data of a missing trial within a trial quadruplet if the other three trials were valid. For each participant, an individual grand mean ERP was computed from the trials of all valid quadruplets, which was then used to linearly interpolate missing data in affected quadruplets. This resulted in an equal number of trials to compute ERP averages for each of the four conditions (hemifield × emotional content), yielding means (±*SD*) of 29.6 ± 3.4 (range 14 to 32) trials per condition. ERP waveforms were low-pass filtered at 12.5 Hz (−24 dB/octave).

2.4. EEG rereferencing and current source density (CSD) transformation

The nose-referenced ERP waveforms (NR) were rereferenced to linked mastoids (average of sites TP9 and TP10; LM) and to the common average of all 72 sites (AR). An infinite reference was estimated via the reference electrode standardization technique (REST) proposed by Yao (2001; Qin et al., 2010). ERP waveforms were transformed into CSD estimates (μV/cm^2 units; 10 cm head radius; 50 iterations; m = 4; smoothing constant $\lambda = 10^{-5}$) using a spherical spline surface Laplacian (Perrin et al., 1989; Kayser and Tenke, 2006a, 2006b; Kayser, 2009). All ERPs in the resulting five data sets were baseline-corrected using the 100 ms preceding stimulus onset. For the time-frequency analyses of these data, the same transformations (LM, AR, REST, CSD) were also applied to the single-trial EEG epochs used to compute the nose-referenced ERPs.

2.5. Principal components analysis for temporal and time-frequency domains

All time-locked epochs for each data transformation (NR, LM, AR, REST, CSD), participant ($N = 130$) and condition (hemifield × emotional content) were imported into EEGlab (version 11.0.3.1b; Delorme and Makeig, 2004) to generate normalized time-frequency averages (function *timef.m*). Event-related spectral perturbations (ERSPs; Makeig, 1993) were computed via fast Fourier transform (FFT) power spectra (zero-padding ratio of 4) relative to the pre-stimulus baseline. Relative increases (synchronization; ERS) and decreases (desynchronization; ERD) in event-related spectral power were quantified by the $\log_{10}$-

[1] The explicit recording of bipolar eye channels is not required when reducing blink artifacts by means of a spatial filter estimated from prototypical EEG intervals, which avoids sacrificing EEG channels in lieu of EOG channels. However, continuous eye activity can still be reconstructed by interpolating EEG activity at scalp locations typically used to differentially record vertical and horizontal eye movements (i.e., at the outer canthi of each eye and at supra- and infraorbital sites). These reconstructed eye traces aid in the evaluation of residual eye movement artifacts.

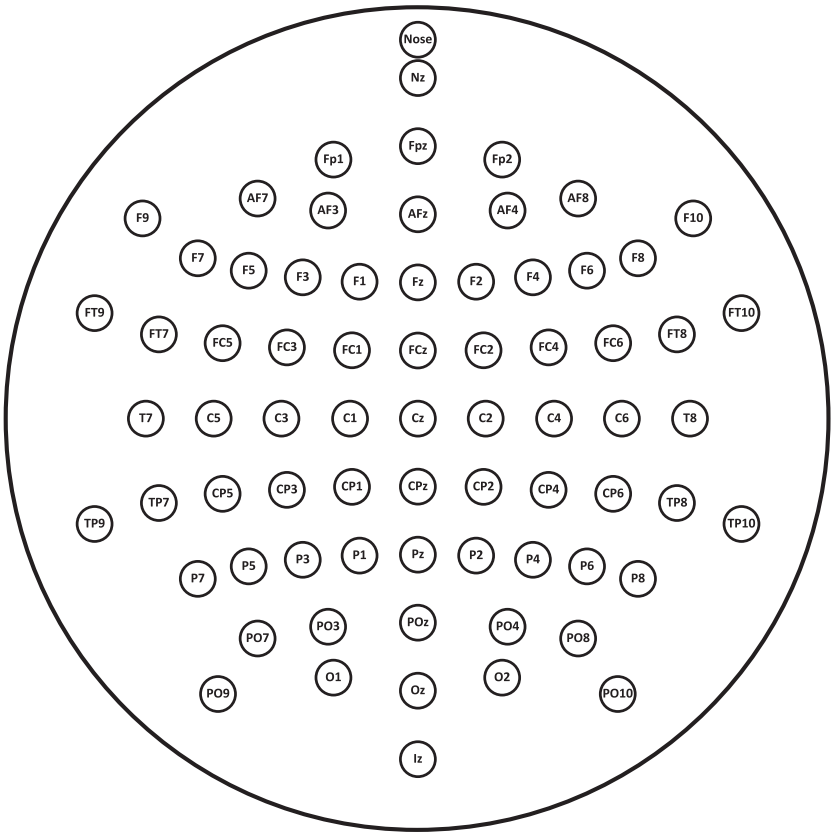

Fig. 1. Layout of extended 10–10 system 72-channel EEG montage (Jurcak et al., 2007).

transformed ratio of overall power and baseline power (multiplied by 10), resulting in normalized ERS/ERD measures (i.e., positive or negative values) for 30 spectral frequencies (1 to 30 Hz) at 256 time points (−75.5 ms to 1175.5 ms) for each participant, condition, and recording site. These frequency-by-time (30-by-256) matrices were further reduced via bilinear interpolation (Matlab function *interp2.m*) to 30-by-82 matrices to adjust the time range of interest (−10 to 800 ms in steps of 10 ms).

Principal components analysis (PCA) was used to determine the common sources of variance of the time domain (i.e., waveforms between −100 and 1000 ms) and time-frequency domain (i.e., 30-by-82 ERSP matrices) data (Kayser and Tenke, 2003; Kayser et al., 2014). To warrant a single PCA decomposition across all data transformations, all five data transformations were first rescaled to the same covariance structure within each domain by using the Eigenvalues of the covariance matrix (i.e., computing the ratio relative to the square root of the sum of the diagonal elements).[2] The rescaled data were then submitted to a single temporal or time-frequency PCA derived from the covariance matrix, followed by unrestricted Varimax rotation of the covariance loadings (Kayser and Tenke, 2003, 2005, 2006c). Using a MatLab function (appendix of Kayser and Tenke, 2003; Matlab code available at http://psychophysiology.cpmc.columbia.edu/erpPCA.html) that emulates BMDP-4 M algorithms (Dixon, 1992), a temporal PCA was computed using 1129 variables (samples in time interval −100 to 1000 ms) and 187,200 observations stemming from 5 data transformations, 130 participants, 4 conditions, and 72 electrode sites. Given the highly-intercorrelated nature of spectral EEG time series data (cf. Kayser et al., 2014) and to reduce computational demands, an analogous time-frequency PCA was computed using 630 variables (ERS/ERD values between 1 and 30 Hz and 0 and 800 ms in steps of 40 ms), effectively reducing the 30-by-82 ERSP matrices to 30-by-21 ERSP matrices, which were rearranged as a vector by concatenating the time vectors for each frequency for each of the 187,200 observations as described above. To interpret the resulting time-frequency factors, their loading vectors were restored to 30-by-21 matrices to create conventional time-frequency plots. The goal of the approach was to derive unbiased, data-driven component measures that effectively characterize N1 amplitude in the time domain, and closely associated event-related oscillations (i.e., delta and/or theta ERS).

2.6. Statistical analysis

For the purpose of the current comparison, it is crucial to avoid any a priori decision of which sites to include in the statistical analysis, which is one predicament when using repeated measures analysis of variance (ANOVA) as the typical method of choice for comparing experimental effects. As another shortcoming of the ANOVA approach, it is always unknown whether all of the assumptions underlying the reference distributions used for parametric *F* statistics are met by the analyzed data. For these reasons, effects of interest (i.e., hemifield-dependent differences in topography) were evaluated by means of randomization distributions estimated from the observed data, which do not depend on any auxiliary assumption (Huo et al., 2013; Maris, 2004). While details of this nonparametric approach are outlined in Kayser et al. (2007), the present analysis focused on characterizing hemifield differences for each data transformation using PCA factors closely linked to N1. This was accomplished by estimating, separately for each data transformation, the

[2] When factoring the covariance matrix, PCA solutions are not affected if the submitted data are rescaled by a constant. For the present data, all transformations were scaled to match the REST covariance structure, resulting in time domain scaling factors of 0.680, 0.790, 1.043 and 0.175 for NR, LM, AR and CSD data transformations, respectively, and 1.040, 1.027, 0.998, and 1.010 for the time-frequency domain. Not surprisingly, for time domain data, ERPs (NR, AR, LM, REST) using identical units (μV) have similar variance compared to CSD-transformed waveforms represented in different units (μV/cm^2), whereas the differences in original data units become obsolete for the log-transformed FFT power ratios (dB) in the time-frequency domain.

maximum randomization distribution (10,000 repetitions) of the univariate (channel-specific) T^2 statistic for paired samples (cf. Eq. 2 in Kayser et al., 2007) after randomly multiplying the observed left/right visual field difference for each participant by +1 or −1. This Scheffé-like post hoc testing procedure controls the family-wise error rate for all channels jointly without any decrease in power that is a consequence of Bonferroni correction (Maris, 2004). Thus, the topographic distribution of significant hemifield differences for each data transformation, as well as the strength of these effects, can be used to compare the statistical impact of these data transformations on hemifield-dependent N1 asymmetries.

Pearson's correlations were used to evaluate associations between the electrophysiological measures (i.e., time vs. time-frequency domain) separately for each data transformation.

After PCA decomposition, data for each visual field was pooled across emotional content. For the purpose of this report, the manipulation of emotional content as well as the clinical assignment of participants as being at low or high risk for major depression, or participants' gender, is irrelevant. These experimental variables are also inconsequential for the employed permutation tests, which evaluate paired (i.e., within-subjects) effects as a function of data transformation.

2.7. Manipulation of noise levels based on sample size

The large sample size conveniently afforded the possibility to systematically manipulate noise levels using smaller subsamples of participants (i.e., considering only the data of 80, 40, 20, or 10 subjects at a time). For the selection of participants into smaller subsamples, 16 bins containing the numbers of all 130 participants were subsequently emptied by random draws of 80 ($16 \times 130 = 2080$, $2080/80 = 26$ draws), 40 ($2080/40 = 52$ draws), 20 ($2080/20 = 104$ draws) or 10 numbers ($2080/10 = 208$ draws). Care was taken so that the same number (participant) was not represented more than once in any given draw, and that all numbers were equally represented across all draws for each sample size (i.e., exactly 16 times). For each draw, permutations tests were performed for the given subsample as done for the total sample (however, using 1000 instead of 10,000 repetitions). For each subsample size, all draws were averaged (i.e., the univariate T^2 statistics) and evaluated at the cumulative randomization distribution (e.g., consisting of $26 \times 1000 = 26{,}000$ max(T^2) values for the subsample size $N = 80$, or $104 \times 1000 = 104{,}000$ for $N = 20$). In this manner, the entire data basis was used for all subsample sizes, effectively evaluating the same visual field difference topographies and hence allowing direct comparisons of statistical effects as a function of sample size.

3. Results

3.1. Time domain

Fig. 2 shows grand mean waveforms at mid-parietooccipital sites (PO3/4) and N1 topographies separately for each of the five data transformations, comparing differences between right and left visual field presentations (see Supplementary Figs. S1–S5 showing grand mean waveforms at all 72 sites for each data transformation). As predicted, a prominent negative deflection peaking at about 125 ms, which was present over the hemisphere contralateral to the stimulated hemifield (i.e., at PO3 with right visual field [RVF] presentations and at PO4 with left visual field [LVF] presentations) but absent over the ipsilateral hemisphere (i.e., at PO3 with LVF and at PO4 with RVF presentations), was observed for all data transformations. This N1 (or N1 sink for CSD data) was most distinct at these mid-parietooccipital sites for all data transformations, although the distinctiveness varied substantially as a function of data transformation. For example, the negativity was notably spread across centroparietal, central, and frontocentral sites for the linked-mastoids reference, and to a lesser degree for the other reference schemes. In contrast, the CSD data revealed a narrow, focal activation of N1 sink that was confined to the mid-parietooccipital region, and also did not transverse to the ipsilateral hemisphere. All data transformation also revealed that N1 inverted in polarity at lateral parieto-occipital sites (PO9/10; cf. also Supplementary Figs. S1–S5), and this inversion was also most distinct and focal for the CSD data. Of note, the average reference enhanced the polarity inversion of N1 while at the same time reducing N1 amplitude, which is a result of averaging the ERP signal across all 72 sites at a time when most dorsal sites are negative (cf. distributed negativity across dorsal sites for all other references). Given that the high signal-to-noise ratio assured the presence of a distinct contralateral N1 in all data transformations, the following analysis centered exclusively on this intended phenomenon.

Fig. 3 shows the first five factor loadings (combined 86.3% explained variance after rotation, each factor > 3%) of the temporal PCA solution stemming from the data of all transformations after rescaling (i.e., equalizing their overall variance).[3] The extracted factor loadings were highly similar when compared to separate PCA solutions derived from the data of each data transformation. Most importantly, the factor with a loading at 127 ms (3.2%) had exactly one counterpart in each of these separate PCA solutions, as evidenced by robust Pearson's correlations of the factor loadings ($.9702 \le r \le .9970$), suggesting that this principal component (i.e., factor *127*) can be employed as an optimal N1 amplitude measure across data transformations.

Fig. 4 shows the corresponding factor score topographies of factor 127 for each data transformation and hemifield, which were highly similar to the grand mean ERP and CSD topographies at 125 ms (cf. Fig. 2). Fig. 4 also shows the respective difference topographies and their non-parametric evaluation via randomization tests. Across all data transformations, the expected hemispheric asymmetries as a function of hemifield were clearly evident. However, compared to all ERP references, the CSD data revealed significant hemifield-dependent differences at mid-parietooccipital sites that were 1) a magnitude larger, 2) locally confined, 3) almost symmetric, and 4) accompanied by significant inversions in polarity at lateral parietooccipital (TPO9/10) and temporoparietal (TP9/10) sites. In contrast, the weaker hemifield-dependent differences for ERPs were also significant at adjacent or even at more remote sites, including left central and frontocentral sites for the nose reference, and less consistent with regard to the polarity inversion at lateral parietooccipital sites. However, despite these striking statistical differences between the five data transformations, all revealed the strongest hemifield-dependent N1 asymmetries at mid-parietooccipital sites.

The impact of increased noise levels is evident from the monotonic decline in statistical significance with reduced sample size, affecting all data transformations equally (see Supplementary Fig. S11 for a comparison of all five sample sizes). As a consequence, the weaker statistical hemifield effects of all ERP references fell outside the conventional 5%-significance threshold for the smallest sample size ($N = 10$), whereas robust effects were still observed for these small subsamples at PO3 and PO4 for the CSD data.

3.2. Time-frequency domain

Fig. 5 shows, separately for each of the five data transformations, the grand mean ERSP plots at mid-parietooccipital sites (PO3/4) and mean early delta/theta ERS (3–5 Hz, 120–200 ms) topographies for each hemifield (see Supplementary Figs. S6–S10 depicting grand mean ERSP plots at all 72 sites for each data transformation). Across transformations, ERSPs were characterized by an early (i.e., approximately 100 to 250 ms) ERS for spectra involving delta and theta frequencies (<8 Hz), which was followed by a prominent alpha ERD (8–15 Hz, 200–650 ms). Notably, both delta/theta ERS and alpha ERD were more robust over the contralateral hemisphere, at least at mid-

[3] A total of 72 factors were extracted and rotated, with 64 explaining less than 1% variance.

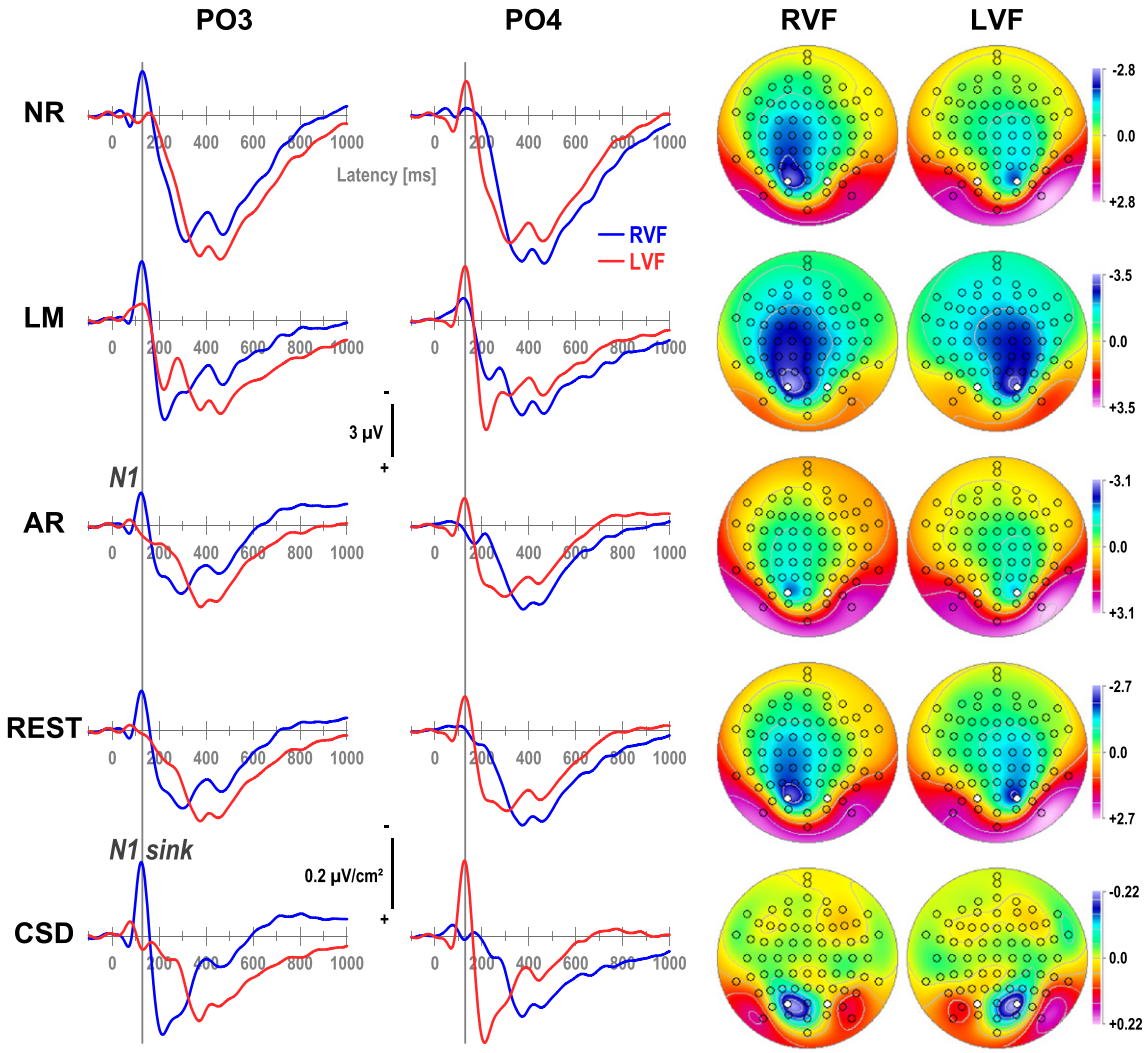

Fig. 2. Grand mean ($N = 130$) ERP [µV] (NR: nose reference; LM: linked-mastoids reference; AR: average reference; REST: reference electrode standardization technique) and surface Laplacian [µV/cm^2] (CSD: current source density) waveforms (−100 to 1000 ms, 100 ms pre-stimulus baseline) comparing stimulus presentations to the right (RVF) or left visual field (LVF) at mid-parieto-occipital sites (PO3/4; locations marked white in maps). Topographies plotted for each hemifield are two-dimensional representations of spherical spline interpolations ($m = 2$; $\lambda = 0$) derived from the corresponding N1 or N1 sink values at 125 ms (indicated by vertical line), using a symmetric scale optimized for each data range.

parietooccipital sites. As with the time domain data, early delta/theta ERS, presumably related to N1, was most distinct for CSD data, which also revealed the strongest hemifield-dependent asymmetries. Whereas the time domain N1 revealed a polarity inversion at lateral parietooccipital sites (PO9/10), the time-frequency data indicated a similar involvement in synchronized low frequencies, further suggesting a close link between N1 and delta/theta ERS. Interestingly, this involvement was enhanced for AR and REST data, but also for NR data, but not for LM and CSD data which consistently revealed maximum delta/theta ERS at mid-parietooccipital sites. Another important observation of these data is that the delta/theta ERS peak latency varies between data transformation, peaking clearly before 200 ms for CSD data for contralateral stimuli, whereas this peak is decidedly later for surface potential data, particularly for NR data. Moreover, whereas delta/theta ERS was largely restricted to posterior sites and early latencies (<300 ms) for CSD data, it was more distributed and extended for surface potential data, particularly for NR and LM data (see Supplementary Figs. S6–S10).[4]

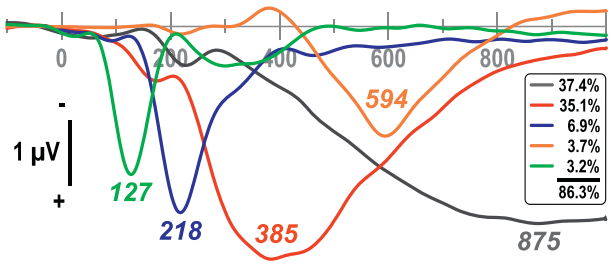

Fig. 3. Factor loadings of the first five temporal PCA (tPCA) factors (>3% explained variance) extracted from ERP (NR, LM, AR, REST) and CSD waveforms ($N = 130$) scaled to REST [µV]. Factor labels reflect the peak latency [ms] of the factor loadings relative to stimulus onset.

Fig. 6 shows the first five factor loadings (combined 41.6% explained variance after rotation, each factor > 3%) of the time-frequency PCA solution stemming from the ERSPs of all data transformations after rescaling.[5] The first factor had prominent factor loadings between 320 and 680 ms within the alpha frequency range, peaking at 480 ms and

[4] These complex relations between N1 amplitude, theta/delta ERS and alpha ERD, and their moderations by data transformation, can be more easily appreciated by comparative animations of the time and time-frequency topographies, which can be obtained at URLs http://psychophysiology.cpmc.columbia.edu/vhf2014.html (all data transformations at 100 samples/s) and http://psychophysiology.cpmc.columbia.edu/vhf2014csd.html (CSD data only at 1000 samples/s).

[5] A total of 371 factors were extracted and rotated, with 346 explaining less than 1% variance.

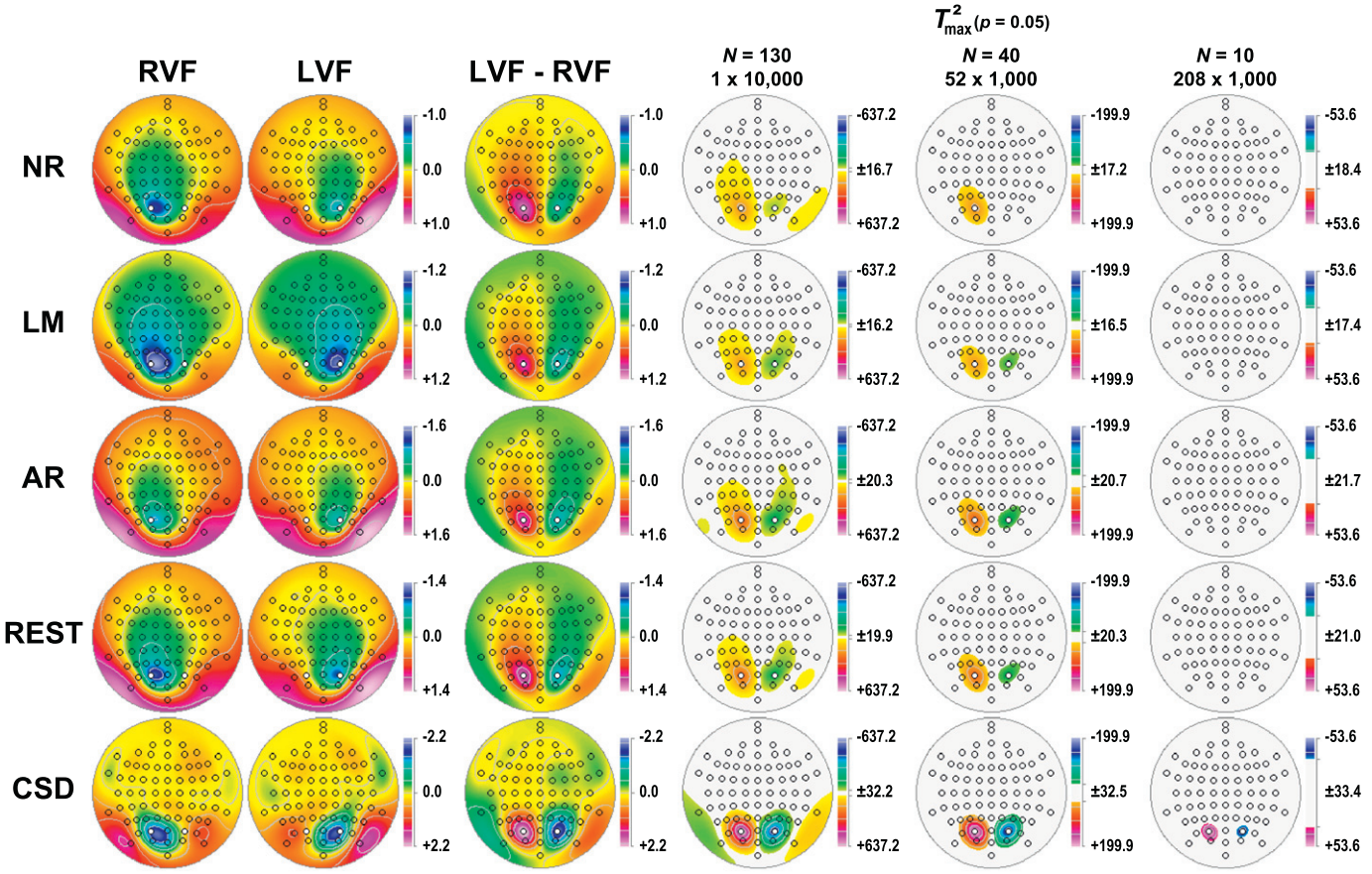

Fig. 4. Statistical evaluation of topographic visual field effects of factor *127* (N1) using randomization tests for paired samples for the full sample ($N = 130$; 10,000 repetitions) and for randomly selected subsamples ($N = 40$, 52 draws; $N = 10$, 208 draws; 1000 repetitions each). Shown are for each data transformation (cf. Fig. 2) the mean factor score topographies for right (RVF) and left (LVF) hemifield presentations and their respective difference, and squared univariate (channel-specific) paired samples *T* statistics thresholded at the 95th quantile ($p = 0.05$) of the corresponding randomization distribution (maximum of all 72-channel squared univariate paired samples *T* statistics). For subsamples, mean T^2 statistics were evaluated with the cumulative randomization distribution resulting from the product of draws and repetitions. To facilitate comparisons of the max(T^2) topographies with the underlying difference topographies, the sign of the difference at each site was applied to the respective T^2 value, which is otherwise always positive. For each data transformation, symmetric scales were optimized for score ranges across RVF and LVF stimuli; however, the same symmetric scale range was used for max(T^2) topographies to allow for better comparison of statistical effects across data transformations. All topographies are two-dimensional representations of spherical spline interpolations ($m = 2$; $\lambda = 0$) derived from the mean factors scores or T^2 statistics available for each recording site.

10 Hz (i.e., labeled *480–10*), and the fourth factor had prominent loadings between 120 and 240 ms and for low frequencies (<8 Hz), peaking at 160 ms and 4 Hz (*160–4*), suggesting that these two factors account for oscillatory variance associated with alpha ERD and delta/theta ERS. As with the time domain PCA, the extracted time-frequency factor loadings were highly similar when compared to separate time-frequency PCA solutions derived from the data of each data transformation, yielding unique factors closely corresponding to factor 480–10 ($.9946 \le r \le .9996$) as well as to factor 160–4 (for NR: $r = .8334$; for LM, AR, REST, CSD: $.9893 \le r \le .9965$).

Fig. 7 shows the factor score topographies of factor 160–4 for each data transformation and hemifield, which were highly comparable to the grand mean early delta/theta ERS topographies (cf. Fig. 5), thereby further bolstering the interpretation of a combined delta/theta ERS factor. The permutation tests performed on the visual field difference topographies for this delta/theta ERS factor (Fig. 7, columns 3 and 4) again revealed significant hemifield-dependent differences at mid-parietooccipital sites for all data transformations, however, those were by a magnitude larger, more focal and more symmetric for CSD data compared to all surface potential transformations. A particular concern was the widespread and asymmetric hemifield-dependent asymmetries observed for NR data.

As with the time-domain data, a monotonic decline in statistical significance accompanied increases in noise levels caused by smaller sample sizes and affected all data transformations equally (see Supplementary Fig. S12 for a comparison of all five sample sizes). For the smallest sample size ($N = 10$), significant hemifield effects survived at PO3 and PO4 for the CSD data, and at PO4 for REST and the linked-mastoids reference.

3.3. Correlations between N1 and delta/theta ERS

For each data transformation, significant associations were found between N1 (tPCA factor 127) and delta/theta ERS (tfPCA factor 160–4) at mid-parietooccipital sites (PO3/4) for the difference between hemifields (Table 1). While the significance of these correlations is of lesser importance given the large sample size ($N = 130$), all correlations were negative, indicating that a relative larger contralateral than ipsilateral N1 (i.e., a negative value) was linked to a relative larger contralateral than ipsilateral delta/theta ERS (i.e., a positive value). This was found for left (PO3) and right (PO4) hemisphere sites, and was even more robust for the hemispheric asymmetry (PO3 minus PO4), clearly indicating that the underlying relationship between synchronized delta and theta activity and N1 amplitude was observed regardless of data transformation. However, the strongest associations were observed for CSD data ($r \ge .6108$), which also revealed rather symmetric associations, in contrast to NR and LM data. The size of these correlations was significantly greater for CSD compared to the four reference schemes at PO3 (versus NR and LM, $p < .05$; versus AR and REST, $p < .10$), at PO4 (versus NR and AR data, $p < .05$; versus REST, $p < .10$), and for the hemispheric asymmetry (versus NR, $p < .05$). Furthermore, NR data also had

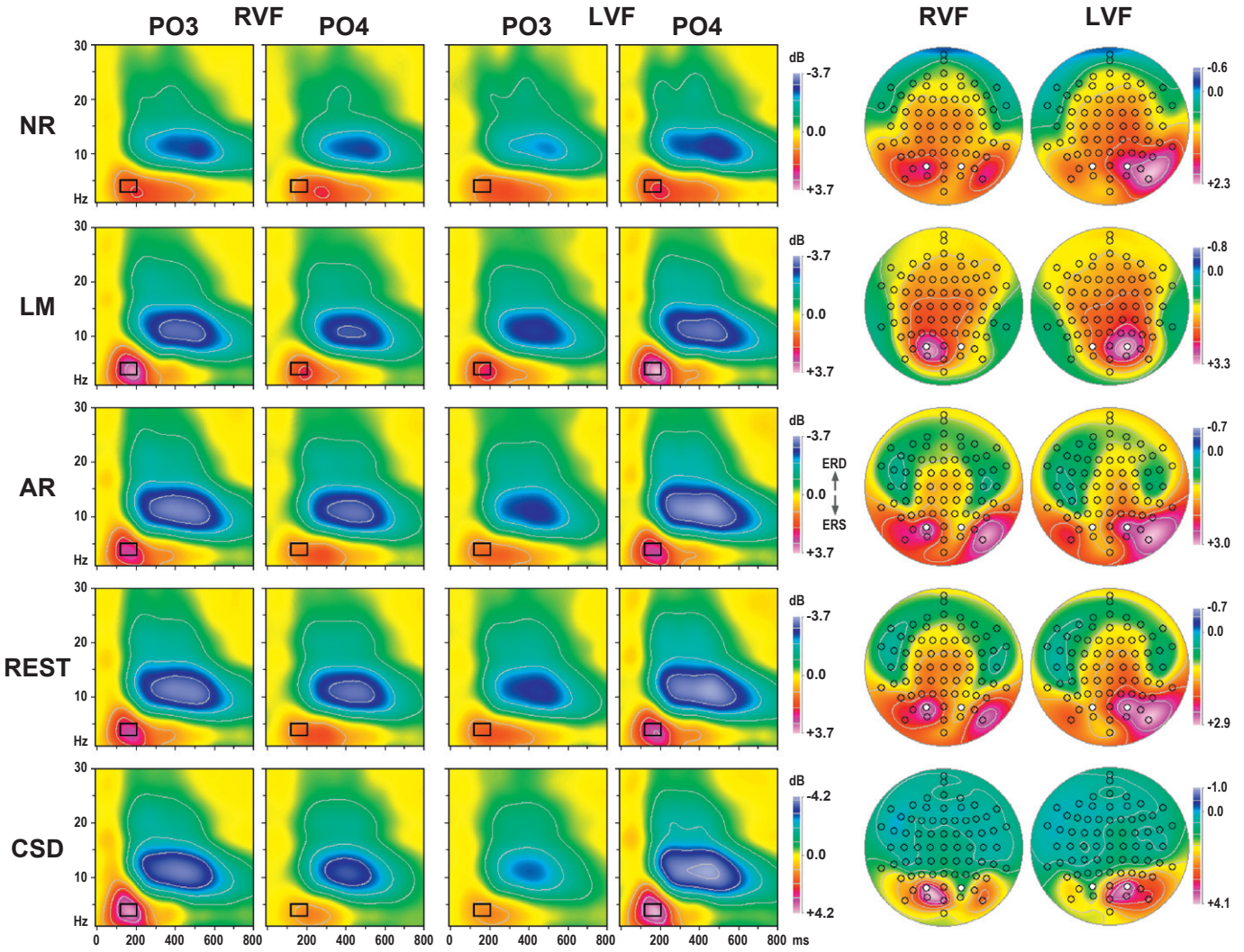

Fig. 5. Grand mean event-related spectral perturbation (ERSP) plots (0 to 800 ms; 1 to 30 Hz) for ERP [μV] (NR, LM, AR, REST) and CSD [μV/cm^2] data comparing stimulus presentations to the right (RVF) or left visual field (LVF) at mid-parieto-occipital sites (PO3/4; locations marked white in maps). Mean ERSP values between 3 and 5 Hz and 120 and 200 ms (indicated by rectangle) reflecting event-related synchronization (ERS) are plotted as topographies for each hemifield using an asymmetric scale optimized for each data range.

significantly weaker associations at PO3 and PO4 compared to the other reference schemes.

3.4. Supplementary analyses for window-based ERP and ERO measures

Although the tPCA and tfPCA factors can be conceived as measures of weighted time window or spectra-by-time window amplitudes (Kayser and Tenke, 2003; Kayser et al., 2014), we also analyzed conventional integrated amplitudes characterizing N1 in time (ERP) and time-frequency (ERO) domains to address whether or not the reported findings are specific to the PCA approach. For each data transformation (no rescaling), mean amplitudes were computed for a symmetric time window around the N1 peak (90–160 ms) and for a combined 100–250 ms time window and 2–6 Hz frequency range (i.e., capturing N1 delta ERS). These conventional ERP and ERO measures were subjected to the same permutations tests used for the PCA-based measures. The findings were fully consistent with the PCA-based results (cf. Supplementary Figs. S13 and S14). The only noticeable difference was a substantial reduction of the overall level of significance (i.e., T^2 maxima were about 55% and 32% smaller for ERP and ERO data, respectively).

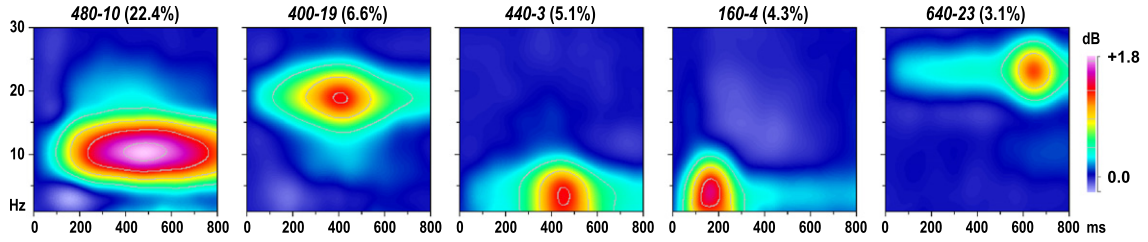

Fig. 6. Factor loadings of the first five time-frequency PCA (tfPCA) factors (>3% explained variance) extracted from the time-frequency ERP (NR, LM, AR, REST) and CSD matrices ($N = 130$) scaled to REST [μV]. Factor labels reflect both peak latency [ms] and peak frequency [Hz] of the factor loadings.

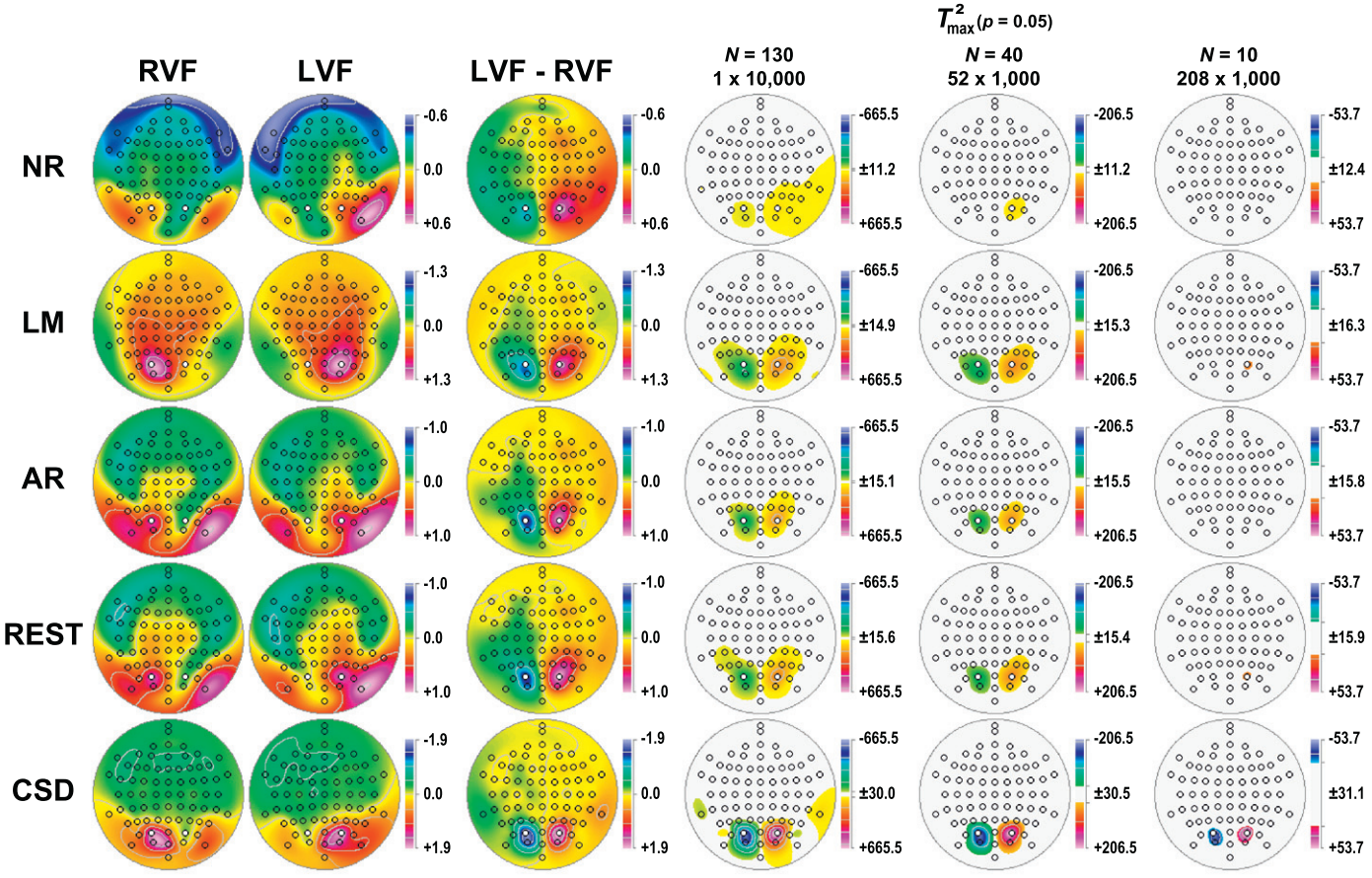

Fig. 7. Statistical evaluation of topographic visual field effects of factor *160–4* (N1 delta ERS) as in Fig. 4.

4. Discussion

4.1. PCA-based findings of ERP and ERO component measures

Using 72-channel EEG recordings with high signal-to-noise ratio obtained from a large sample ($N = 130$), this study evaluated hemifield-dependent ERPs (N1) and ERSPs (theta/delta ERS) as a function of EEG recording reference (nose, linked mastoids, average, REST) and their reference-free surface Laplacian transform (CSD) by means of temporal and time-frequency PCA and randomization tests. A robust negativity peaking at about 125 ms after stimulus onset was the most prominent early waveform deflection for all data transformations, and was also largest at posterior sites (PO3/4) contralateral to the stimulated hemifield (N1pc). For surface potentials, however, N1pc also spread to other recording sites in anterior direction, presumably due to volume conduction, although the extent of spreading depended on the particular reference scheme (greatest for nose, less for linked mastoids). In stark contrast, CSD-based N1pc sinks were restricted to contralateral posterior sites. Furthermore, spreading of N1pc toward anterior sites was strongly asymmetric for the nose reference (LH > RH), somewhat asymmetric for the average reference but in opposite direction (RH > LH), fairly symmetric for linked mastoids and REST, and strongly symmetric for CSD. All of these effects were significant, however, the CSD effects were a magnitude stronger than those of the surface potentials. Given the known involvement of contralateral extrastriate cortex in the generation of N1pc (e.g., Clark et al., 1995), the strength and symmetry of the CSD effects must be considered an accurate representation of the underlying radial current flow at scalp. The effects not only have a weaker representation in the ERPs, but ERPs may also render spurious effects that may lead to invalid conclusions.

These hemifield-dependent N1pc asymmetries were paralleled by a transient ERS spanning theta and delta frequencies and peaking at about 160 ms after stimulus onset. The topographical maximum of the time-frequency component was at the same contralateral posterior sites

Table 1
Pearson's correlations between N1 and delta/theta ERS for hemifield differences (RVF–LVF) at mid-parietooccipital sites for each data transformation and corresponding pairwise comparisons of significant differences (p value).

Data transformation	PO3	PO4	PO3–PO4
NR	−0.2328 [a]	−0.3281	−0.5114
LM	−0.4063	−0.5647	−0.6286
AR	−0.4813	−0.4862	−0.5642
REST	−0.4706	−0.5162	−0.5971
CSD	−0.6108	−0.6380	−0.6604
Comparison [b]			
NR vs. CSD	0.0001	0.0005	0.0341
LM vs. CSD	0.0131		
AR vs. CSD	0.0697	0.0373	
REST vs. CSD	0.0560	0.0716	
NR vs. REST	0.0146	0.0332	
LM vs. REST			
AR vs. REST			
NR vs. AR	0.0110	0.0646	
LM vs. AR			
NR vs. LM	0.0611	0.0086	0.0823

Note. N1 as measured by temporal PCA factor 127, delta/theta ERS as measured by time-frequency factor 160–4 ($N = 130$). NR: nose reference; LM: linked-mastoids reference; AR: average reference; REST: reference electrode standardization technique; CSD: current source density; RVF: right visual field; LVF: left visual field; PO3–PO4: hemisphere asymmetry.

[a] $p = .0077$, all other correlations, $p \leq .0001$.

[b] Pairwise significant differences (after Fisher z-transformation of each correlation) with $p < .10$ are detailed.

(PO3/4) for CSD and linked-mastoid data, but over neighboring lateral-inferior parietal sites for the other surface potential transformations; still, the respective hemifield difference topographies revealed the strongest differential theta/delta ERS activations at PO3 and PO4 for all data transformations. As for N1pc, the CSD effects were by far more robust, focal and symmetric than those observed for the surface potentials. The close association between N1pc and theta/delta ERS was further bolstered by substantial correlations between the two measures for all data transformations, however, with again the CSD data revealing the strongest and most symmetric relationship. This affinity between a stimulus-locked increase of theta and delta CSD power over precisely the same scalp regions assumed to generate visual N1 sink amplitude closely matched findings for bilateral auditory N1 sinks during a three-stimulus oddball task, which also corresponded to CSD-based delta/theta ERS at the same sites, implicating auditory cortex activation over each hemisphere (Kayser et al., 2014).

These ERP and ERO[6] findings of early EEG activations in a well-understood experimental paradigm underscore a superior performance of the surface Laplacian compared to all surface potential transformations. Granted that not all possible EEG reference schemes were included in the present comparison (e.g., unilateral ear lobe, vertex, or any other), it nevertheless seems highly improbable that a different reference would have yielded substantially improved results, because volume conduction appears to be the common underlying problem affecting all surface potentials (cf. Tenke and Kayser, 2012). Still, there were notable differences among the four EEG reference schemes, indicating that the nose is a rather poor choice compared to the three other references, at least for the current paradigm. In this regard, the relative good performance of the linked mastoids reference, which by definition yields a residual polarity reversal at these lateral inferior temporal–parietal sites after removal of their common EEG signal (i.e., for each sample point, TP9 and TP10 have identical values with opposite polarity), may be exactly due to the nature of the visual half-field paradigm because the 'virtual' reference location will maximize the targeted hemisphere asymmetries (cf. Saron and Davidson, 1989, who also found improved estimates of visual interhemispheric transfer time with a linked-ears compared to a mid-frontal reference). This interpretation is consistent with simulations and conclusions by Nunez et al. (1997) when using a digitally linked-ears reference, suggesting that a linked-mastoids reference cancels some of the volume conduction effects at large distances.

Somewhat surprisingly, there were only subtle differences between the average reference and REST, which may be due to the comparatively dense EEG montage combined with a high signal-to-noise ratio of ERP and ERO measures and excellent statistical power (cf. Hagemann et al., 2001). Previous comparisons showing favorable performance of REST over the average and other references have focused on less stable EEG measures (coherence and default mode network spectral power; Qin et al., 2010; see also comments by Nunez, 2010) or less robust methods of spectral or ERP component quantification (i.e., a priori frequency bands and peak-based amplitudes as opposed to PCA-based measures; Yao et al., 2005, 2007). While it has been noted that different EEG references may be more or less useful for different research objectives (e.g., Dien, 1998; Wolpaw and Wood, 1982), or it has been proposed to consider several reference schemes as a design factor when analyzing EEG data when lacking consensus for the 'best' reference (e.g., Allen et al., 2004), such considerations seem moot given that a simple data transformation yields unambiguous measures that 1) unify all possible reference schemes, 2) more directly reflect neuronal activation meant to be studied in the first place, 3) are easier to interpret, and 4) reveal stronger statistical effects.

[6] In a strict sense, ERSP measures do not necessarily quantify true oscillations. Despite this conceptual limitation, ERPs and ERSPs are both event-related and each domain can illuminate and extend our understanding of the other (i.e., time or time-frequency).

4.2. Signal-to-noise ratio

Despite the widespread notion that surface Laplacian estimates are inherently more susceptible to increases in noise levels (e.g., Bradshaw and Wikswo, 2001), the present comparisons across data transformations were not affected by sample size. Rather, the overall level of statistical significance was increasingly reduced with increasingly smaller sample sizes, virtually affecting all data transformations equally. Thus, in this paradigm, the surface Laplacian still outperformed all reference schemes, independent of the particular noise level. One may argue that the hemifield task itself produced a high signal-to-noise ratio, yielding a contralateral N1 enhancement in every participant, and even if not, then certainly by averaging the statistical outcome across many smaller subsamples, the strong signal will prevail and favor the CSD transform. But such an argumentation becomes circular because a reliable identification of true effects is (or should be) the paramount scientific objective. Moreover, these findings are consistent with evidence showing that the surface Laplacian compares favorably to other data transformations (i.e., average and linked-earlobes reference) when the signal-to-noise ratio is reduced by limiting the number of EEG epochs to 10 in a speeded reaction time task used to study error-related, mid-frontal negativities (Cohen, 2014).

In hindsight, these present observations, while impressive and informative, may not come as a surprise when keeping in mind that the surface Laplacian is a linear transformation (e.g., Tenke and Kayser, 2012). For this reason, the superior performance of CSD measures for the full sample will equally hold for any subsample (i.e., as long as the same data are compared across data transformations). As another consideration, the CSD transformation itself may suppress (unsystematic) noise, particularly when it is based on spherical splines employing a more rigid spline flexibility (i.e., a constant of $m = 4$ used for the present data, as opposed to $m = 3$ or $m = 2$; cf. Perrin et al., 1989; Kayser and Tenke, in revision).

4.3. Impact of quantification method

Using integrated time and time-frequency windows as a more conventional approach for ERP and ERO component quantification did not alter the comparative findings observed for PCA-based measures. However, overall significance levels were substantially reduced across all data transformations when employing window-based amplitudes, confirming previous evidence that PCA-based measures show favorable statistical properties compared to conventional component measures, including larger effect sizes (e.g., Beauducel et al., 2000; Beauducel and Debener, 2003; Kayser et al., 1998). As argued previously (Kayser and Tenke, 2003), Varimax-rotated temporal PCA components can be conceived as a measure of weighted time window amplitude that avoids the subjectivity of selecting time intervals. The same applies to frequency and time-frequency PCA, where the components can be conceived as weighted amplitude spectra (i.e., across a narrow frequency band; Tenke and Kayser, 2005) or weighted spectra-by-time window amplitudes (Kayser et al., 2014). As it turns out, these data-driven measures also summarize EEG/ERP data better than conventional a priori or post hoc measures.

A well-known problem with temporal PCA is its insensitivity to latency variation (e.g., Möcks, 1986). It may therefore be argued that a PCA factor may not optimally measure N1pc peaks, which may vary considerably across participants and conditions (in this case, left versus right hemifield), and peak-based measures, accounting for both amplitude and latency, may constitute a more precise (i.e., better) alternative. While the problem of latency jitter can be addressed by aligning CSD waveforms, which are characterized by a large and steep visual N1, with respect to their peak latency to render an improved PCA-based N1 amplitude measure (Kayser et al., 2012), this issue is only a concern for the present analysis inasmuch as latency jitter may have differentially affected the different data transformations; however, this does not

appear to be the case (cf. Fig. 2 showing virtually the same mean N1 peak latency at sites PO3/4 for *all* data transformations). It seems therefore prudent to assume that any latency jitter problems may have equally affected all data transformations.

We sought to employ PCA methods as a superior, less biased approach for ERP and ERO data analysis compared to traditional strategies, especially peak-based measures. For the present objective, peak amplitudes fail to generate complete topographies because 1) N1 inverts across sites, 2) often no clear peak can be identified for a given participant, condition or site, and 3) peaks differ between data transformations, rendering a systematic topographic comparison moot. Even more relevant is the implicit assumption that distinct ERP deflections (i.e., peaks) provide "precise" information. However, this cannot not be true because ERP peaks change in time and space when changing the reference. This contrasts with peaks derived from waveform differences between sites (note: not between conditions or groups), which are unaffected by the choice of reference — this invariant topographic information is precisely what is reflected by the surface Laplacian transform (cf. Kayser and Tenke, in revision). The specific manner of component quantification (PCA, ICA, integrated amplitude, peak amplitude or latency, etc.) is unrelated to the surface Laplacian transformation, so if differences in peak latency are the primary research objective, the surface Laplacian should also provide more precise and reliable results compared to surface potentials (cf. Burle et al., 2015).

4.4. Limitations, generalizations, and conclusions

Although our intention was to showcase the profitable characteristic of the surface Laplacian for electrophysiologic research when directly compared to the corresponding scalp potentials, a considerable limitation of this comparative study is its reliance on a prototypical test case, as the current findings cannot necessarily be generalized to other paradigms and EEG measures. For example, one may argue that certain EEG rhythms or later cognitive ERP components, such as P3 or other subcomponents of the late positive complex, originate from the contributions of multiple neuronal generators, which are inadequately represented in CSD-transformed surface potentials. These concerns need to be tested with comparative forward simulation studies[7] (e.g., Tenke and Kayser, in revision; Tenke and Kayser, 2012), which indicate that while the overall signal amplitude for deep versus shallow sources may be indeed relatively smaller for CSD than field potential data, the signal-to-noise ratio is nevertheless superior for the surface Laplacian. These empirical findings seem to contradict the common notion that CSDs mainly represent shallow (i.e., cortical) brain activity but are by comparison to field potentials fairly insensitive to deep (i.e., subcortical) neuronal generators (Perrin et al., 1987). This notion has resulted in the general recommendation to employ surface Laplacian and surface potentials in tandem (e.g., Giard et al., 2014; Nunez and Srinivasan, 2006; Srinivasan et al., 1998). However, the present data strongly indicate that not only were the CSD peak maxima substantially stronger than those of surface potentials but that the shallower fall-off of the scalp potentials as a result of volume conduction (i.e., less signal attenuation with increasing distance) resulted in incorrect representations of brain activity. Therefore, the current test case does not suggest any added advantage of using field potentials as a supplement to the reference-free surface Laplacian.

Considering that evidence presented was only derived from a single, rather specific ERP paradigm, can these findings nevertheless be generalized to other cognitive tasks and components? Is a surface Laplacian always "better" and what is "better"? From a theoretical perspective, a surface Laplacian is reference-free, constitutes a unique transformation (i.e., there is only *one* CSD), and has unambiguous polarity. These advantages are presumed to be offset by a loss of information attributed to the spatial filter properties of the surface Laplacian, which would affect signals of low spatial frequency (i.e., generated by deep and distributed sources; e.g., Nunez and Srinivasan, 2006). However, deep generators have very little practical impact on cognitive electrophysiology because cortical sources dominate the EEG recorded at scalp. The major advantage of the hemifield paradigm is that the functional neuroanatomy involving the activation of the contralateral visual cortex is well understood and not a matter of interpretation. While surface potentials may have larger amplitudes across the EEG/ERP topography, these larger amplitudes do not necessarily reflect a genuine signal, and are plainly wrong at more anterior sites for the present data. Thus, "better" is an accurate representation of the true signal and favorable statistical properties for measuring it. The assumption that the comparison between surface potential and surface Laplacian measures will somehow reverse just because things get murkier (i.e., more and distributed neuronal generators, lower signal-to-noise ratio, late cognitive as opposed to early stimulus-driven components), implying that substantive information is lost in the data transformation under these circumstances, does not seem to be parsimonious, and, more importantly, nor is it backed by empirical evidence.

To the contrary, in agreement with the present findings and their interpretation are previous comparisons of nose-referenced late cognitive ERPs and their CSD counterparts observed during auditory oddballs tasks, which did not provide any evidence in support of concerns that the CSD measures are inadequate for the representation of (deep) generator sources underlying a broadly-distributed parietal P3 (Kayser and Tenke, 2006a). We also note that the present observations are entirely consistent with the simulations reported by Nunez et al. (1997), which revealed a virtual absence of erroneous correlations between scalp sites for all interelectrode distances. This was in striking contrast to scalp potentials, which manifested profound erroneous EEG signal correlations at close or distant locations, dependent of the EEG reference scheme, which is attributable to both volume conduction and reference electrode location. Noting that the spatial filter properties of a surface Laplacian are responsible for yielding accurate representations for many neocortical dynamic behaviors, Nunez et al. (1997) nevertheless suggested that scalp potentials and surface Laplacians are complementary and partly independent measures of brain activation, because the latter may filter out sources with very low spatial frequencies. Unfortunately, the implication of this has often been to disregard surface Laplacian methods and instead to exclusively rely on scalp potentials for EEG analysis, implicitly shifting the burden of proof to those researchers who employ CSD methodology, whereas it should be the other way around. The arbitrariness of the EEG reference, its associated error in representing neuronal activity, and the negative consequences of volume conduction appear to outweigh by far the theoretical disadvantages when using a surface Laplacian. For these reasons, we argue that the current findings are indeed a good representative example of the adverse consequences of volume conduction, which are inherent to surface potentials, obscuring a bona fide representation of neuronal activation patterns at scalp that directly reflect regional brain activity. However, their most accurate recognition and quantification is the ultimate goal of cognitive neuroscience using electrophysiologic methods.

Supplementary data to this article can be found online at http://dx.doi.org/10.1016/j.ijpsycho.2014.12.011.

Acknowledgments

This research was supported in part by grant MH036197 from the National Institute of Mental Health (NIMH) awarded to Myrna M. Weissman. Time-frequency CSD–PCA methods were developed under the umbrella of NIMH grant MH094356. We greatly appreciate the assistance of Karen Abraham, Dan M. Alschuler, Jorge E. Alvarenga, Jamie Skipper, and Virginia Warner with recruitment and data collection.

[7] A notorious problem of simulation studies is the adequate implementation of realistic noise, which depends on EEG signal properties and recording characteristics (e.g., montage density, etc.).

Waveform plotting software was written by Charles L. Brown, III. We are deeply indebted to Dezhong Yao for generously providing the C++ source code to generate the REST lead field matrix. Finally, we are grateful for the helpful comments of two anonymous reviewers, which prompted the statistical evaluation of noise levels caused by differences in sample size and of window-based amplitude measures.

References

Allen, J.J., Coan, J.A., Nazarian, M., 2004. Issues and assumptions on the road from raw signals to metrics of frontal EEG asymmetry in emotion. Biol. Psychol. 67 (1–2), 183–218.

Alschuler, D.M., Tenke, C.E., Bruder, G.E., Kayser, J., 2014. Identifying electrode bridging from electrical distance distributions: a survey of publicly-available EEG data using a new method. Clin. Neurophysiol. 125 (3), 484–490.

Beauducel, A., Debener, S., 2003. Misallocation of variance in event-related potentials: simulation studies on the effects of test power, topography, and baseline-to-peak versus principal component quantifications. J. Neurosci. Methods 124 (1), 103–112.

Beauducel, A., Debener, S., Brocke, B., Kayser, J., 2000. On the reliability of augmenting/reducing: peak amplitudes and principal components analysis of auditory evoked potentials. J. Psychophysiol. 14 (4), 226–240.

Bertrand, O., Perrin, F., Pernier, J., 1985. A theoretical justification of the average reference in topographic evoked potential studies. Electroencephalogr. Clin. Neurophysiol. 62 (6), 462–464.

BioSemi, Inc., 2001. ActiveTwo-multichannel, DC amplifier, 24-bit resolution, biopotential measurement system with active electrodes. Author, Amsterdam, NL (http://www.biosemi.com).

Bradshaw, L.A., Wikswo Jr., J.P., 2001. Spatial filter approach for evaluation of the surface Laplacian of the electroencephalogram and magnetoencephalogram. Ann. Biomed. Eng. 29 (3), 202–213.

Bryson, S.E., McLaren, J., Wadden, N.P., MacLean, M., 1991. Differential asymmetries for positive and negative emotion: hemisphere or stimulus effects? Cortex 27 (3), 359–365.

Burle, B., Spieser, L., Roger, C., Casini, L., Hasbroucq, T., Vidal, F., 2015. Spatial and temporal resolution of EEG: is it really black and white? A scalp current density view. Int. J. Psychophysiol. 97 (3), 210–220 (in this issue).

Carvalhaes, C.G., de Barros, J.A., 2015. The surface Laplacian technique in EEG: theory and methods. Int. J. Psychophysiol. 97 (3), 174–188 (in this issue).

Casiraghi, M., Fortier-Gauthier, U., Sessa, P., Dell'Acqua, R., Jolicoeur, P., 2013. N1pc reversal following repeated eccentric visual stimulation. Psychophysiology 50 (4), 351–364.

Clark, V.P., Fan, S., Hillyard, S.A., 1995. Identification of early visual evoked potential generators by retinotopic and topographic analyses. Hum. Brain Mapp. 2 (3), 170–187.

Cohen, M.X., 2014. Comparison of different spatial transformations applied to EEG data: a case study of error processing. Int. J. Psychophysiol. http://dx.doi.org/10.1016/j.ijpsycho.2014.09.013 (2014 Oct 20, [Epub ahead of print]).

Delorme, A., Makeig, S., 2004. EEGLAB: an open source toolbox for analysis of single-trial EEG dynamics including independent component analysis. J. Neurosci. Methods 134 (1), 9–21.

Dien, J., 1998. Issues in the application of the average reference: review, critiques, and recommendations. Behav. Res. Methods Instrum. Comput. 30 (1), 34–43.

Dixon, W.J. (Ed.), 1992. BMDP Statistical Software Manual: To Accompany the 7.0 Software Release. University of California Press, Berkeley, CA.

Donchin, E., Heffley, E.F., 1978. Multivariate analysis of event-related potential data: a tutorial review. In: Otto, D.A. (Ed.), *Multidisciplinary Perspectives in Event-Related Brain Potential Research. Proceedings of the Fourth International Congress on Event-Related Slow Potentials of the Brain (EPIC IV)*, Hendersonville, NC, April 4–10, 1976, The Office, Washington, DC, pp. 555–572.

Eimer, M., 1996. The N2pc component as an indicator of attentional selectivity. Electroencephalogr. Clin. Neurophysiol. 99 (3), 225–234.

Endrass, T., Mohr, B., Rockstroh, B., 2002. Reduced interhemispheric transmission in schizophrenia patients: evidence from event-related potentials. Neurosci. Lett. 320 (1–2), 57–60.

Ferree, T.C., 2006. Spherical splines and average referencing in scalp electroencephalography. Brain Topogr. 19 (1–2), 43–52.

Giard, M.H., Besle, J., Aguera, P.E., Gomot, M., Bertrand, O., 2014. Scalp current density mapping in the analysis of mismatch negativity paradigms. Brain Topogr. 27 (4), 428–437.

Gruber, W.R., Klimesch, W., Sauseng, P., Doppelmayr, M., 2005. Alpha phase synchronization predicts P1 and N1 latency and amplitude size. Cereb. Cortex 15 (4), 371–377.

Hagemann, D., Naumann, E., Thayer, J.F., 2001. The quest for the EEG reference revisited: a glance from brain asymmetry research. Psychophysiology 38 (5), 847–857.

Herrmann, C.S., Rach, S., Vosskuhl, J., Strüber, D., 2014. Time-frequency analysis of event-related potentials: a brief tutorial. Brain Topogr. 27 (4), 438–450.

Huo, M., Heyvaert, M., Van den Noortgate, W., Onghena, P., 2013. Permutation tests in the educational and behavioral sciences: a systematic review. Methodology 1–17 http://dx.doi.org/10.1027/1614-2241/a000067 (2013 May 13, [Online first publication]).

Junghöfer, M., Elbert, T., Tucker, D.M., Braun, C., 1999. The polar average reference effect: a bias in estimating the head surface integral in EEG recording. Clin. Neurophysiol. 110 (6), 1149–1155.

Jurcak, V., Tsuzuki, D., Dan, I., 2007. 10/20, 10/10, and 10/5 systems revisited: their validity as relative head-surface-based positioning systems. Neuroimage 34 (4), 1600–1611.

Kayser, J., 2003. Polygraphic Recording Data Exchange — PolyRex. Department of Biopsychology, New York State Psychiatric Institute (http://psychophysiology.cpmc.columbia.edu/PolyRex.htm).

Kayser, J., 2009. Current source density (CSD) interpolation using spherical splines — CSD toolbox (Version 1.1). Division of Cognitive Neuroscience, New York State Psychiatric Institute (http://psychophysiology.cpmc.columbia.edu/Software/CSDtoolbox).

Kayser, J., Tenke, C.E., 2003. Optimizing PCA methodology for ERP component identification and measurement: theoretical rationale and empirical evaluation. Clin. Neurophysiol. 114 (12), 2307–2325.

Kayser, J., Tenke, C.E., 2005. Trusting in or breaking with convention: towards a renaissance of principal components analysis in electrophysiology. Clin. Neurophysiol. 116 (8), 1747–1753.

Kayser, J., Tenke, C.E., 2006a. Principal components analysis of Laplacian waveforms as a generic method for identifying ERP generator patterns: I. Evaluation with auditory oddball tasks. Clin. Neurophysiol. 117 (2), 348–368.

Kayser, J., Tenke, C.E., 2006b. Principal components analysis of Laplacian waveforms as a generic method for identifying ERP generator patterns: II. Adequacy of low-density estimates. Clin. Neurophysiol. 117 (2), 369–380.

Kayser, J., Tenke, C.E., 2006c. Consensus on PCA for ERP data, and sensibility of unrestricted solutions. Clin. Neurophysiol. 117 (3), 703–707.

Kayser, J., Tenke, C.E., 2006d. Electrical distance as a reference-free measure for identifying artifacts in multichannel electroencephalogram (EEG) recordings. Psychophysiology 43, S51 (http://psychophysiology.cpmc.columbia.edu/mmedia/spr2006/ElecDistArti.pdf).

Kayser, J., Tenke, C.E., 2010. In search of the Rosetta Stone for scalp EEG: converging on reference-free techniques. Clin. Neurophysiol. 121 (12), 1973–1975.

Kayser, J., Tenke, C.E. 2015. Issues and considerations for using the scalp surface Laplacian in EEG/ERP research: a tutorial review. Int. J. Psychophysiol. (in revision).

Kayser, J., Tenke, C., Nordby, H., Hammerborg, D., Hugdahl, K., Erdmann, G., 1997. Event-related potential (ERP) asymmetries to emotional stimuli in a visual half-field paradigm. Psychophysiology 34 (4), 414–426.

Kayser, J., Tenke, C.E., Bruder, G.E., 1998. Dissociation of brain ERP topographies for tonal and phonetic oddball tasks. Psychophysiology 35 (5), 576–590.

Kayser, J., Bruder, G.E., Tenke, C.E., Stewart, J.E., Quitkin, F.M., 2000. Event-related potentials (ERPs) to hemifield presentations of emotional stimuli: differences between depressed patients and healthy adults in P3 amplitude and asymmetry. Int. J. Psychophysiol. 36 (3), 211–236.

Kayser, J., Tenke, C.E., Gates, N.A., Bruder, G.E., 2007. Reference-independent ERP old/new effects of auditory and visual word recognition memory: joint extraction of stimulus- and response-locked neuronal generator patterns. Psychophysiology 44 (6), 949–967.

Kayser, J., Tenke, C.E., Kroppmann, C.J., Alschuler, D.M., Fekri, S., Gil, R., Jarskog, L.F., Harkavy-Friedman, J.M., Bruder, G.E., 2012. A neurophysiological deficit in early visual processing in schizophrenia patients with auditory hallucinations. Psychophysiology 49 (9), 1168–1178.

Kayser, J., Tenke, C.E., Kroppmann, C.J., Alschuler, D.M., Ben David, S., Fekri, S., Bruder, G.E., Corcoran, C.M., 2013. Olfaction in the psychosis prodrome: electrophysiological and behavioral measures of odor detection. Int. J. Psychophysiol. 90 (2), 190–206.

Kayser, J., Tenke, C.E., Kroppmann, C.J., Alschuler, D.M., Fekri, S., Ben-David, S., Corcoran, C.M., Bruder, G.E., 2014. Auditory event-related potentials and alpha oscillations in the psychosis prodrome: neuronal generator patterns during a novelty oddball task. Int. J. Psychophysiol. 91 (2), 104–120.

Keil, A., Debener, S., Gratton, G., Junghöfer, M., Kappenman, E.S., Luck, S.J., Luu, P., Miller, G.A., Yee, C.M., 2014. Committee report: publication guidelines and recommendations for studies using electroencephalography and magnetoencephalography. Psychophysiology 51 (1), 1–21.

Klimesch, W., Schack, B., Schabus, M., Doppelmayr, M., Gruber, W., Sauseng, P., 2004. Phase-locked alpha and theta oscillations generate the P1–N1 complex and are related to memory performance. Brain Res. Cogn. Brain Res. 19 (3), 302–316.

Makeig, S., 1993. Auditory event-related dynamics of the EEG spectrum and effects of exposure to tones. Electroencephalogr. Clin. Neurophysiol. 86 (4), 283–293.

Makeig, S., Westerfield, M., Jung, T.P., Enghoff, S., Townsend, J., Courchesne, E., Sejnowski, T.J., 2002. Dynamic brain sources of visual evoked responses. Science 295 (5555), 690–694.

Maris, E., 2004. Randomization tests for ERP topographies and whole spatiotemporal data matrices. Psychophysiology 41 (1), 142–151.

Marzetti, L., Nolte, G., Perrucci, M.G., Romani, G.L., Del Gratta, C., 2007. The use of standardized infinity reference in EEG coherency studies. Neuroimage 36 (1), 48–63.

McFarland, D.J., 2014. The advantages of the surface Laplacian in brain–computer interface research. Int. J. Psychophysiol. http://dx.doi.org/10.1016/j.ijpsycho.2014.07.009 (2014 Aug 1, [Epub ahead of print]).

McKeever, W.F., 1986. Tachistoscopic methods in neuropsychology. In: Hannay, J.H. (Ed.), Experimental Techniques in Human Neuropsychology. Oxford University Press, New York, pp. 167–211.

Möcks, J., 1986. The influence of latency jitter in principal component analysis of event-related potentials. Psychophysiology 23 (4), 480–484.

NeuroScan, Inc., 2003a. SCAN 4.3 — Vol. II. EDIT 4.3 — Offline analysis of acquired data (*Document number 2203, Revision D*). Compumedics Neuroscan, El Paso, TX.

NeuroScan, Inc., 2003b. STIM^2 User Guide (*Document number 9027, Revision A*). Compumedics Neuroscan, El Paso, TX.

Nunez, P.L., 2010. REST: a good idea but not the gold standard. Clin. Neurophysiol. 121 (12), 2177–2180.

Nunez, P.L., Srinivasan, R., 2006. Electric fields of the brain: the neurophysics of EEG. Oxford University Press, New York.

Nunez, P.L., Westdorp, A.F., 1994. The surface Laplacian, high resolution EEG and controversies. Brain Topogr. 6 (3), 221–226.

Nunez, P.L., Srinivasan, R., Westdorp, A.F., Wijesinghe, R.S., Tucker, D.M., Silberstein, R.B., Cadusch, P.J., 1997. EEG coherency. I: statistics, reference electrode, volume conduction, Laplacians, cortical imaging, and interpretation at multiple scales. Electroencephalogr. Clin. Neurophysiol. 103 (5), 499–515.

Nunez, P.L., Silberstein, R.B., Shi, Z., Carpenter, M.R., Srinivasan, R., Tucker, D.M., Doran, S.M., Cadusch, P.J., Wijesinghe, R.S., 1999. EEG coherency II: experimental comparisons of multiple measures. Clin. Neurophysiol. 110 (3), 469–486.

Pascual-Marqui, R.D., Gonzalez-Andino, S.L., Valdes-Sosa, P.A., Biscay-Lirio, R., 1988. Current source density estimation and interpolation based on the spherical harmonic Fourier expansion. Int. J. Neurosci. 19 (3–4), 237–249.

Perrin, F., Bertrand, O., Pernier, J., 1987. Scalp current density mapping: value and estimation from potential data. IEEE Trans. Biomed. Eng. 34 (4), 283–288.

Perrin, F., Pernier, J., Bertrand, O., Echallier, J.F., 1989. Spherical splines for scalp potential and current density mapping [Corrigenda EEG 02274, EEG Clin. Neurophysiol., 1990, 76, 565]. Electroencephalogr. Clin. Neurophysiol. 72 (2), 184–187.

Pfurtscheller, G., Lopes da Silva, F.H., 1999. Event-related EEG/MEG synchronization and desynchronization: basic principles. Clin. Neurophysiol. 110 (11), 1842–1857.

Pivik, R.T., Broughton, R.J., Coppola, R., Davidson, R.J., Fox, N., Nuwer, M.R., 1993. Guidelines for the recording and quantitative analysis of electroencephalographic activity in research contexts. Psychophysiology 30 (6), 547–558.

Qin, Y., Xu, P., Yao, D., 2010. A comparative study of different references for EEG default mode network: the use of the infinity reference. Clin. Neurophysiol. 121 (12), 1981–1991.

Saron, C.D., Davidson, R.J., 1989. Visual evoked potential measures of interhemispheric transfer time in humans. Behav. Neurosci. 103 (5), 1115–1138.

Springer, S.P., Deutsch, G., 1981. Left brain, right brain. Freeman & Company, San Francisco.

Srinivasan, R., Tucker, D.M., Murias, M., 1998. Estimating the spatial Nyquist of the human EEG. Behav. Res. Methods Instrum. Comput. 30 (1), 8–19.

Tenke, C.E., Kayser, J., 2001. A convenient method for detecting electrolyte bridges in multichannel electroencephalogram and event-related potential recordings. Clin. Neurophysiol. 112 (3), 545–550.

Tenke, C.E., Kayser, J., 2005. Reference-free quantification of EEG spectra: combining current source density (CSD) and frequency principal components analysis (fPCA). Clin. Neurophysiol. 116 (12), 2826–2846.

Tenke, C.E., Kayser, J., 2012. Generator localization by current source density (CSD): implications of volume conduction and field closure at intracranial and scalp resolutions. Clin. Neurophysiol. 123 (12), 2328–2345.

Tenke, C.E., Kayser, J. 2015. Surface Laplacians and phase properties of EEG rhythms: simulated generators in a volume-conduction model. Int. J. Psychophysiol. (in revision).

Thuraisingham, R.A., 2011. Analytical expressions for the transfer matrix to standardize scalp potentials to infinity reference. J. Comput. Neurosci. 31 (3), 609–613.

Van der Haegen, L., Cai, Q., Stevens, M.A., Brysbaert, M., 2013. Interhemispheric communication influences reading behavior. J. Cogn. Neurosci. 25 (9), 1442–1452.

Verleger, R., Zurawska Vel Grajewska, B., Jaskowski, P., 2012. Time-course of hemispheric preference for processing contralateral relevant shapes: P1pc, N1pc, N2pc, N3pc. Adv. Cogn. Psychol. 8 (1), 19–28.

Weissman, M.M., Warner, V., Wickramaratne, P., Moreau, D., Olfson, M., 1997. Offspring of depressed parents. 10 years later. Arch. Gen. Psychiatry 54 (10), 932–940.

Weissman, M.M., Wickramaratne, P., Nomura, Y., Warner, V., Verdeli, H., Pilowsky, D.J., Grillon, C., Bruder, G., 2005. Families at high and low risk for depression: a 3-generation study. Arch. Gen. Psychiatry 62 (1), 29–36.

Weissman, M.M., Wickramaratne, P., Nomura, Y., Warner, V., Pilowsky, D., Verdeli, H., 2006. Offspring of depressed parents: 20 years later. Am. J. Psychiatry 163 (6), 1001–1008.

Whitford, T.J., Kubicki, M., Ghorashi, S., Schneiderman, J.S., Hawley, K.J., McCarley, R.W., Shenton, M.E., Spencer, K.M., 2011. Predicting inter-hemispheric transfer time from the diffusion properties of the corpus callosum in healthy individuals and schizophrenia patients: a combined ERP and DTI study. Neuroimage 54 (3), 2318–2329.

Wolpaw, J.R., Wood, C.C., 1982. Scalp distribution of human auditory evoked potentials. I. Evaluation of reference electrode sites. Electroencephalogr. Clin. Neurophysiol. 54 (1), 15–24.

Yao, D., 2001. A method to standardize a reference of scalp EEG recordings to a point at infinity. Physiol. Meas. 22 (4), 693–711.

Yao, D., Wang, L., Oostenveld, R., Nielsen, K.D., Arendt-Nielsen, L., Chen, A.C., 2005. A comparative study of different references for EEG spectral mapping: the issue of the neutral reference and the use of the infinity reference. Physiol. Meas. 26 (3), 173–184.

Yao, D., Wang, L., Arendt-Nielsen, L., Chen, A.C., 2007. The effect of reference choices on the spatio-temporal analysis of brain evoked potentials: the use of infinite reference. Comput. Biol. Med. 37 (11), 1529–1538.

Young, A.W., 1982. Methodological and theoretical bases of visual hemifield studies. In: Beaumont, J.D. (Ed.), Divided visual field studies of cerebral organization. Academic Press, London, pp. 11–27.